Electronic Supplementary Material (ESI) for Materials Advances.

Supporting information

Exploring the Electrocatalytic Prowess of Synergistic 1T-MoS_2 -Metallic Ni Composite Towards Alkaline Hydrogen Evolution

Avishek Roy[a], *Ayan Mondal*[#a], *Harish Reddy Inta*[#a,b], *Sourav Ghosh*[a], *Khushboo S Paliwal*[a], *Soumalya Debnath*[a], *Ajith Ambattuparambil Valsan*[a] *and Venkataramnan Mahalingam*[a]*

[a]Department of Chemical Science, Indian Institute of Science Education and Research (IISER)

Kolkata, Mohanpur, West Bengal 741246, India

[b]Department of Energy Science & Engineering, Daegu Gyeongbuk Institute of Science & Technology (DGIST), Daegu 42988, South Korea

[#] Equal Contribution

Email: mvenkataramanan@yahoo.com

Contents

Number of pages : 26

Number of Figures : 35

Number of Tables : 6

1. Experimental Section:

1.1 Materials: Ammonium heptamolybdate Hexahydrate ($(NH_4)_6Mo_7O_{24}\cdot 6H_2O$), Potassium Hydroxide (KOH), Ethylene Glycol (EG) were purchased from Merck. Thiourea (CH_4N_2S) and Hydrazine hydrate were obtained from Spectrochem. Pvt. Ltd. Mumbai, India. Nickel (II) chloride Hexahydrate ($NiCl_2\cdot 6H_2O$) was purchased from Sisco Research Laboratories. Pvt. Ltd. Ethanol (EtOH) was obtained from Changshu Hongsheng Fine Chemical Co. Ltd. Nafion and Carbon paper was purchased from Alfa Aesar and Fuel Cell store, respectively. Further, all the chemicals (analytical grade) were used for further purification.

1.2 Synthesis of Materials:

1.2.1 *Syn*thesis of 1T-MoS_2: 1T-MoS_2 was synthesized under Solvothermal conditions using ammonium heptamolybdate hexahydrate ($(NH_4)_6Mo_7O_{24}\cdot 6H_2O$) and thiourea as a precursor. Initially, 300 mg $(NH_4)_6Mo_7O_{24}\cdot 6H_2O$ was added to 50 ml distilled water and stirred for about 5 mins. After that, 1g thiourea was introduced and stirred for 5 mins. Subsequently, the entire reaction mixture was transferred to the 200 ml Teflon container, which was enveloped with a steel jacket. The steel jacket was transferred to the typical hydrothermal reaction setup and heated at 180°C for 24 h. Eventually, the container was allowed to cool down naturally, and the black color product was obtained. This product was washed twice with distilled water and methanol by centrifugation (at 10000 rpm for 5 mins each time) and dried under Vacuum.

1.2.2 Synthesis of Ni nanowire: Ni nanowire was synthesized under wet chemical conditions. 36 mg aqueous solution of $NiCl_2\cdot 6H_2O$ (in 1 ml distilled water) was added to 14 ml ethylene glycol in a 100 ml round bottom flask and stirred well for 1 hour. After that, the mixture was heated at about 110°C in an oil bath for the next 15 minutes. After that, 1.5 ml hydrazine hydrate was introduced to the hot mix and continued to warm at 110°C without stirring for the next 1 hour. The resultant black color product was immediately floating over the solution. Subsequently, the product was washed twice with distilled water and methanol by centrifugation (at 9000 rpm for 5 min each time) and dried under Vacuum.

1.2.3 Synthesis of 1T-MoS_2 - Ni(X) composites: For the preparation of composite structure, initially, 30 mg of 1T-MoS_2 was dispersed in 14 ml ethylene glycol medium in a 100 ml round bottom flask. The resultant solution was sonicated well to mix the 1T-MoS_2 and glycol better. After that, different amounts of aqueous solutions of $NiCl_2\cdot 6H_2O$ (9, 18, 27, 36 mg) (in 1 ml aqueous distilled water) were added to the dispersed MoS_2 solution and sonicated for the next 5 mins. Then, the entire reaction mixture was stirred for about 1 hour for good mixing between individual 1T-MoS_2

and Ni residues. Subsequently, the resultant mixture was heated at about 110°C in an oil bath for the next 15 min. Subsequently, 1.5 ml hydrazine hydrate was introduced to the hot reaction mixture and continued to be heated at 110°C for 1 hour with continuous stirring. Finally, the black color product was obtained, which was washed twice with distilled water and methanol through centrifugation (at 10000 rpm for 5 mins each time) and dried under Vacuum. The corresponding products are denoted as 1T-MoS_2 – Ni (9), 1T-MoS_2 – Ni (18), 1T-MoS_2 – Ni (27), and 1T-MoS_2 – Ni (36).

1.2.4 Synthesis of NiS: NiS was synthesized under typical hydrothermal reaction conditions. Initially, 36 mg (0.15 mmol) $NiCl_2 \cdot 6H_2O$ solution (in 1 ml water) was added to 14 ml ethylene glycol. The resultant solution was stirred well for 5 mins for better mixing. After that, 23 mg (0.3 mmol) of thiourea was introduced into the reaction container and stirred well. Subsequently, 1.5 ml of hydrazine hydrate was added to the reaction mixture and stirred well for 2-3 mins. The reaction mixture was then transferred into the 50 ml Teflon container, enveloped with a steel jacket, and heated at 180°C for 24 h in an air oven. Eventually, the container was allowed to cool down naturally, and the black color product was obtained. Finally, the black color product was washed twice with distilled water and methanol by centrifugation (at 10000 rpm for 5 mins each time) and was dried under Vacuum.

2. Material characterization:

The structural property of the materials was analyzed by Powder X-ray diffraction technique (PXRD) using Rigaku Mini flex diffractometer with Cu Kα (λ = 0.154 nm) as a radiation source (operating at 40 kV) in the 2θ range 5 to 80 ° with the Scan rate of 5°/min. The PXRD of post-electrode material was analyzed on carbon paper substrate with a scan rate of 2°/min. Fourier transform infrared spectroscopy (FTIR) determined the functional groups in the material using a PerkinElmer RX1 spectrometer equipped with the KBr disk technique. To understand the phase of as-prepared materials, Raman spectroscopy was performed using a Micro Raman Spectrometer (Horiba Jobin Yvon, HR 800 double grating). The chemical state of the elements in the as-prepared materials was analyzed by X-ray Photoelectron Spectroscopy (XPS, PHI 5000 Versa Probe IV, ULVAC-PHI Inc., USA) equipped with monochromatic Al-Kα X-Ray source (hν = 1486.6 eV). Further, the survey scans were analyzed using an X-ray pass energy of 225 eV. The High-resolution XPS spectra of the major elements were recorded using 55 eV pass energy. The XPS raw data were analyzed using Casa XPS software. The XPS of post-electrode materials was recorded on carbon paper substrate. To probe the microstructure of the materials, HR-TEM (High-resolution transmission electron microscope) (JEOL, JSM-2100F microscope) operating at 200 kV and Field

Emission Scanning electron microscopy (FESEM) (ZEISS SUPRA 55 VP JSM) were performed. The FESEM was equipped with energy-dispersive X-ray Spectroscopy (EDS) of GEMINI column technology. Prior to the HRTEM & FESEM analyses, the samples were well dispersed in methanol and drop-cast on a carbon-coated copper grid and silicon wafer substrate, respectively.

3. Electrochemical Measurements:

A conventional three-electrode system was used for all electrochemical measurements using SP-300 Biologic Science Instrument. The Ag/AgCl (in 3.5M KCl) was used as a reference electrode and the Graphite rod was used as a counter electrode. Further, for the execution of a prolonged stability test, Hg/HgO is used as a reference electrode.

3.1 Details of working electrode preparation:

The working electrode was prepared using the drop-casting technique. Initially, 2 mg catalyst powder was dispersed in 200 µl of EtOH, then 40 µl polymeric binder Nafion solution was added. The resultant dispersion was sonicated well for 10 mins and drop-casted onto 0.5 x 0.5 cm^2 carbon paper with 120 µl of total catalyst ink (60 µl each side of carbon paper). Finally, the loading of the catalyst material was maintained at 4 mg/cm^2, which was held constant for the rest of the samples. All electrochemical measurements were performed using 1M KOH Solution at room temperature.

3.2 Alkaline HER performance study:

Prior to the HER measurements, the contribution from dissolved oxygen current was avoided by continuous purging with argon (Ar) gas. All the electrochemical performances of the working electrodes were initially calculated using Ag/AgCl as reference electrode and finally, all the potential was corrected with respect to RHE obeying the following equations 1 and 2:

$$E(RHE) = E\,(Ag/AgCl) + 0.230 + 0.059\ pH \quad \text{---------- (1)}$$

$$E\,(RHE) = E\,(Ag/AgCl) + 0.230 + 0.059 \times 14 \quad (pH \approx 14 \text{ for 1M KOH}) \quad \text{---------- (2)}$$

Before evaluating electrochemical HER activity, the electrode material was preconditioned for 20 cyclic voltammetry (CV) cycles between the voltage window of 0 to (- 0.3) Vs RHE to obtain a steady voltammetric current response. The scan rate was fixed to 50 mV/s. Thereafter, HER activity was monitored by calculating the overpotential value from (100% manually iR Corrected) backward CV within the same voltage window at a low scan rate of 5 mV/s. The overpotential (η) value was estimated utilizing the following equation 3 :

(For HER thermodynamic potential is 0 V) $\eta = E\,(RHE) - 0$ ---------- (3)

Tafel slope was calculated from the Tafel plot (overpotential (η) vs log|current density (j)|) using 100% manually iR-corrected backward LSV curve. The Tafel plot was obtained by fitting the η Vs logj plot obeying the Tafel equation $\eta = a + b \log(j/j_0)$. Here b represents the corresponding tafel slope, j and j_0 represent geometric current density and exchange current density, respectively. To understand the electrochemical active surface area (ECSA), electrochemical double layer capacitance (C_{dl}) was estimated by measuring the CV by varying scan rates (ν) ranging (between 5 to 100 mV/s) at open circuit potential (OCP). The ECSA was calculated using the following equation (4 and 5):

$$i = \nu \times C_{dl} \quad \text{----------(4)}$$

$$ECSA = Cdl / C_s \quad \text{----------(5)}$$

Where i denotes scan rate dependent total double layer current at non-faradaic region, the C_s designates the specific capacitance. The electrochemical impedance analysis was performed in the AC frequency range of 1Hz to 100 kHz.

3.3 Alkaline OER performance study:

The electrochemical OER activity was evaluated from the 100% iR-corrected backward LSV curve.

The overpotential value at 10 mA/cm^2_{geo} was recorded using the following equation 6.

(For OER thermodynamic potential is 1.23V) $\eta = E\ (RHE) - 1.23$ ----------(6)

Tafel slope was determined from 100% iR corrected backward LSV curve.

3.4 Overall water-splitting performance:

The alkaline electrolyzer was constructed using 1T-MoS_2-Ni(18) as (-ve) and NiS as (+ve) electrodes, respectively. The polarization curve of the overall cell was recorded in the two-electrode configuration within the voltage window of 1 to 2 V.

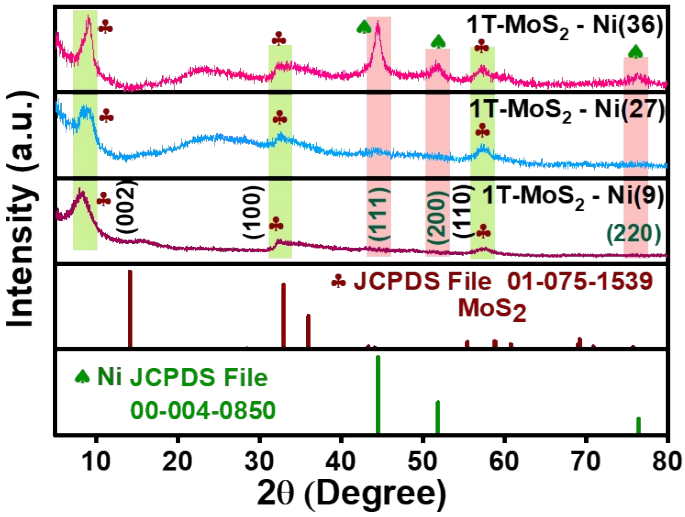

Figure S1: PXRD pattern of other 1T-MoS_2-Ni(X) (X= 9, 18, 36 mg) composite materials along with a standard pattern of metallic Ni (JCPDS File #00-004-0850) and MoS_2 (JCPDS File #01-075-1539)

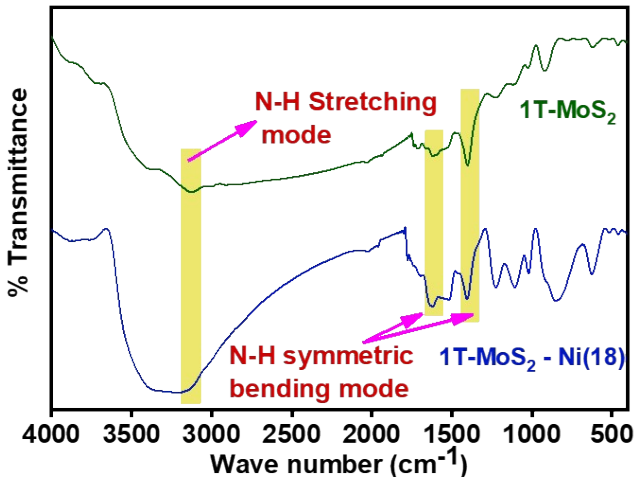

Figure S2: FTIR analysis of 1T-MoS_2 and 1T-MoS_2-Ni(18) composite material with N-H bending and stretching.

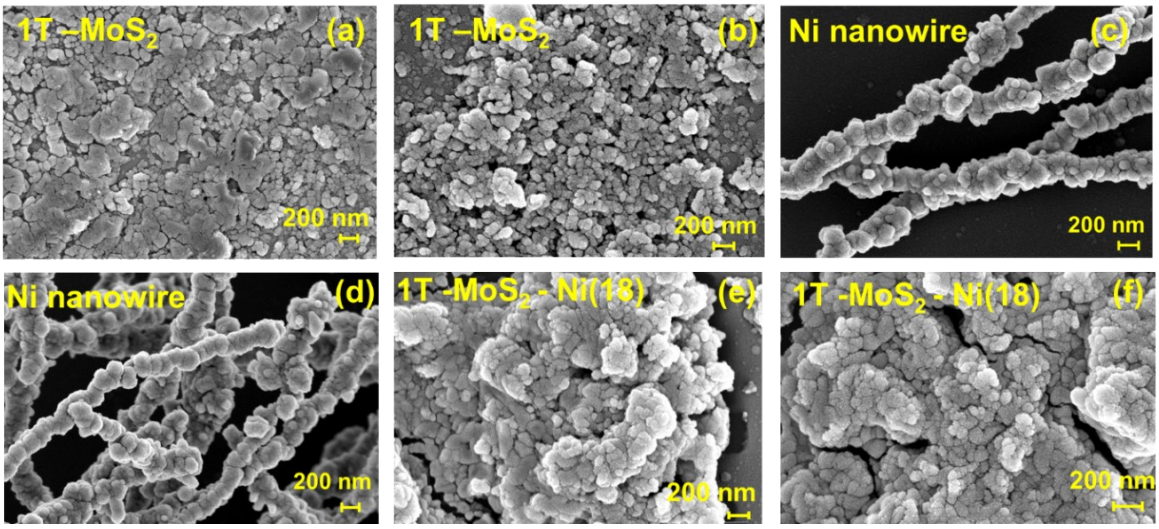

Figure S3: FESEM images of as-prepared (a, b) 1T-MoS_2, (c, d) Ni nanowire, (e, f) 1T-MoS_2-Ni(18).

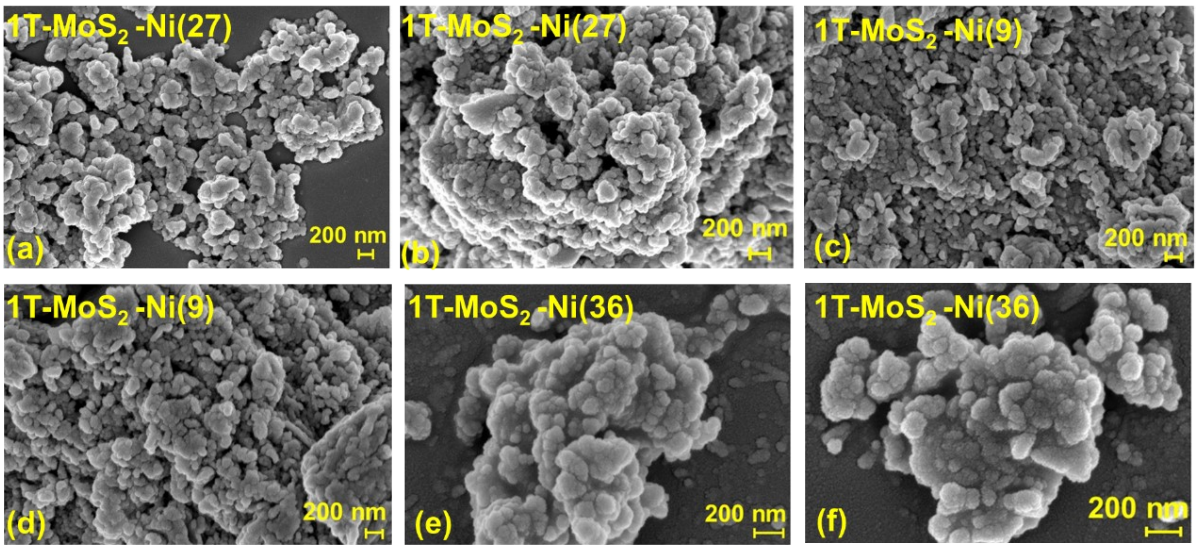

Figure S4: FESEM images of different composite materials (a, b) 1T-MoS_2-Ni(27), (c, d) 1T-MoS_2-Ni(9), (e, f) 1T-MoS_2-Ni(36).

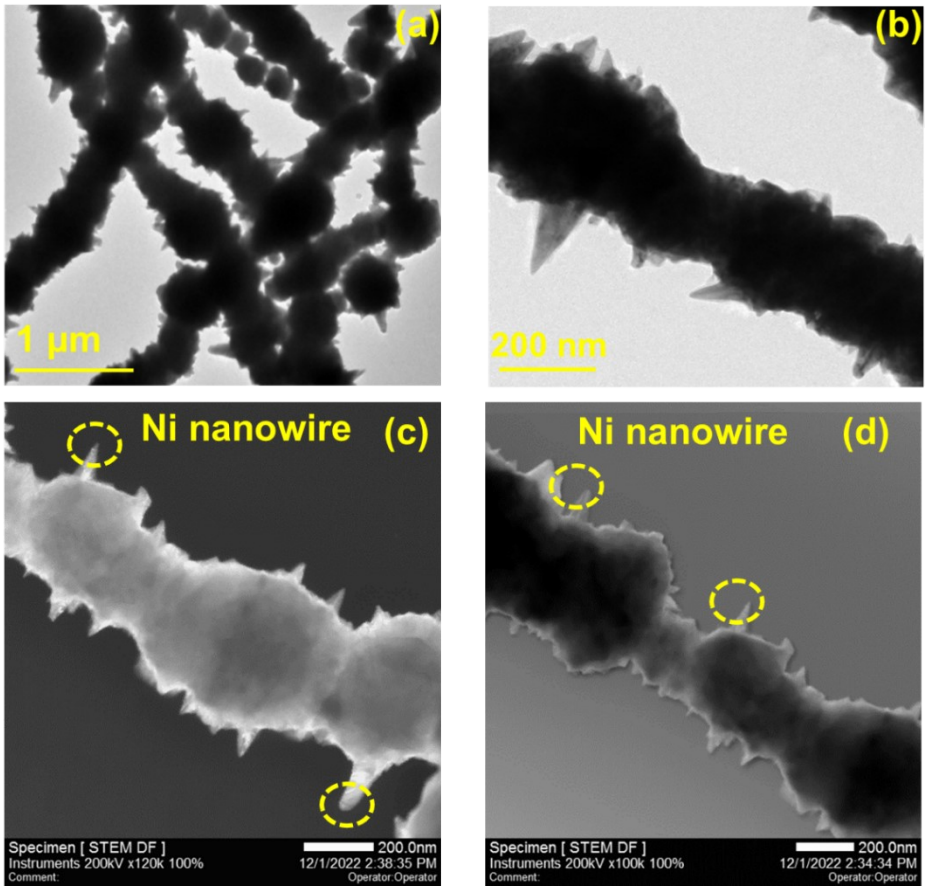

Figure S5: (a, b) TEM images, (c, d) STEM images of Ni nanowire.

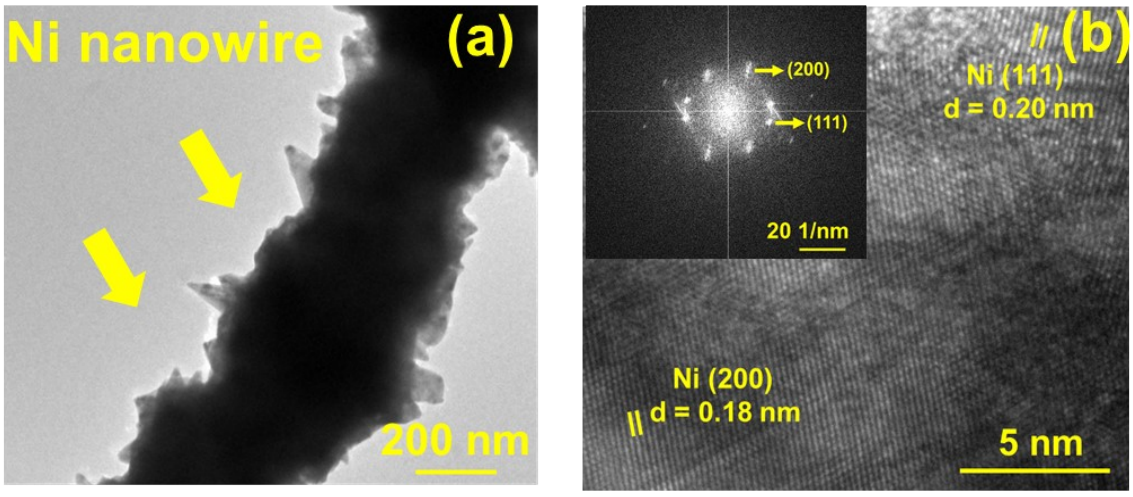

Figure S6: (a) TEM image, (b) HRTEM analysis of the as-prepared Ni nanowire. (Inside the Figure b, the corresponding FFT pattern is displayed)

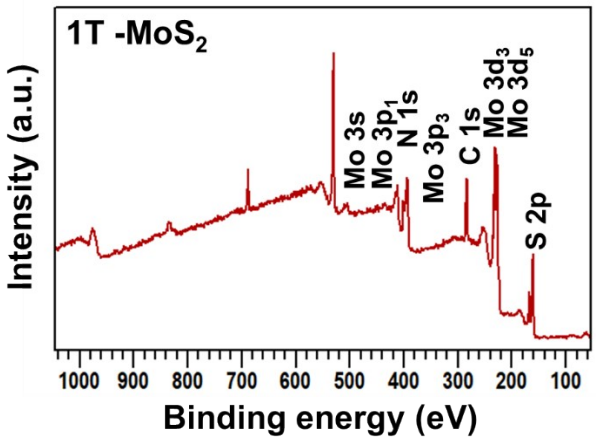

Figure S7: XPS survey scan of 1T-MoS_2.

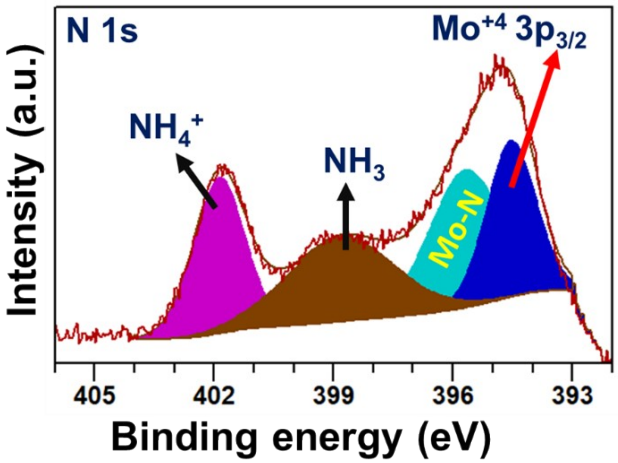

Figure S8: The deconvoluted high-resolution N 1s XPS spectrum of 1T-MoS_2.

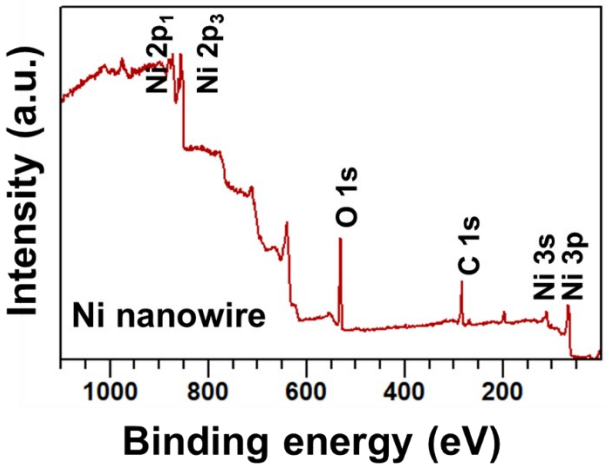

Figure S9: XPS survey scan of metallic Ni nanowire.

Table S1: XPS peak positions of as-synthesized metallic Ni nanowire.

$Ni^0(2p_{3/2})$	$Ni^0(2p_{1/2})$	$Ni^{+2}(2p_{3/2})$	$Ni^{+2}(2p_{1/2})$	Satellite	satellite
852 eV	869.2 eV	855.3 eV	873 eV	861 eV	879.3 eV

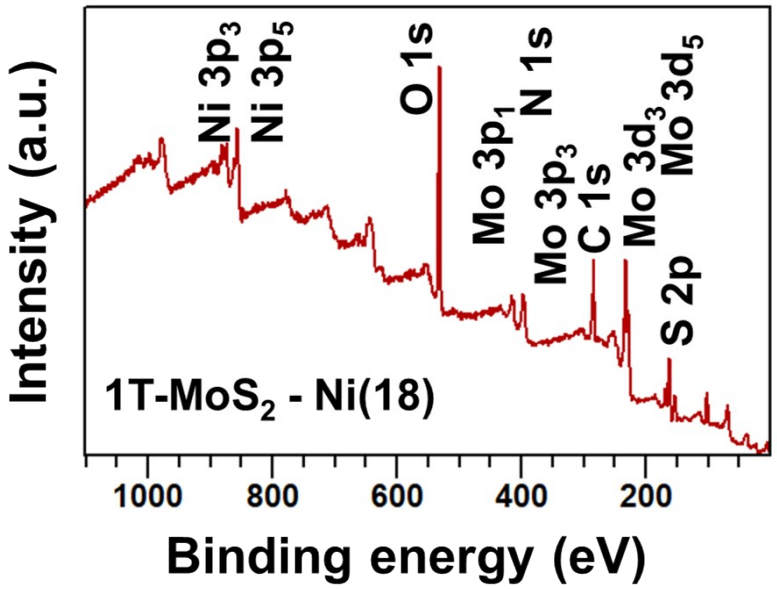

Figure S10: XPS survey scan of 1T-MoS_2-Ni(18) composite material.

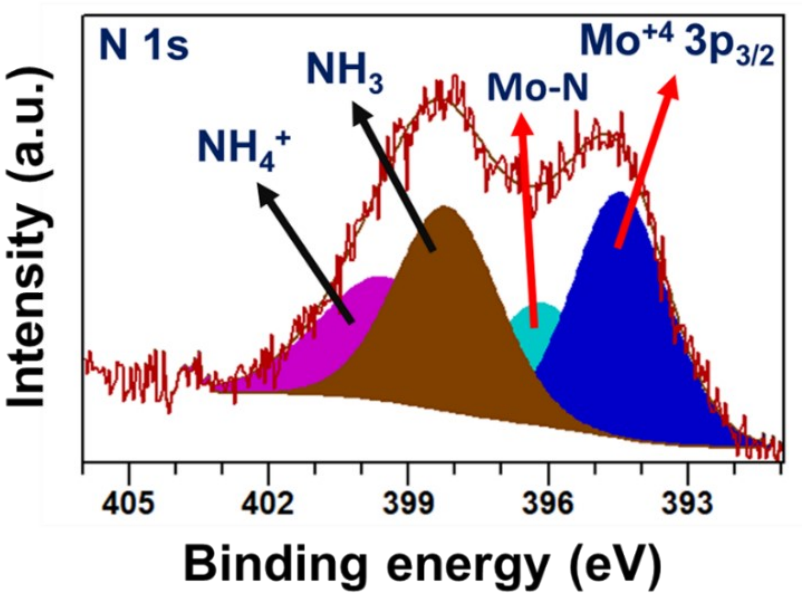

Figure S11: The deconvoluted high-resolution XPS spectrum of N 1s for 1T-MoS_2-Ni(18) composite.

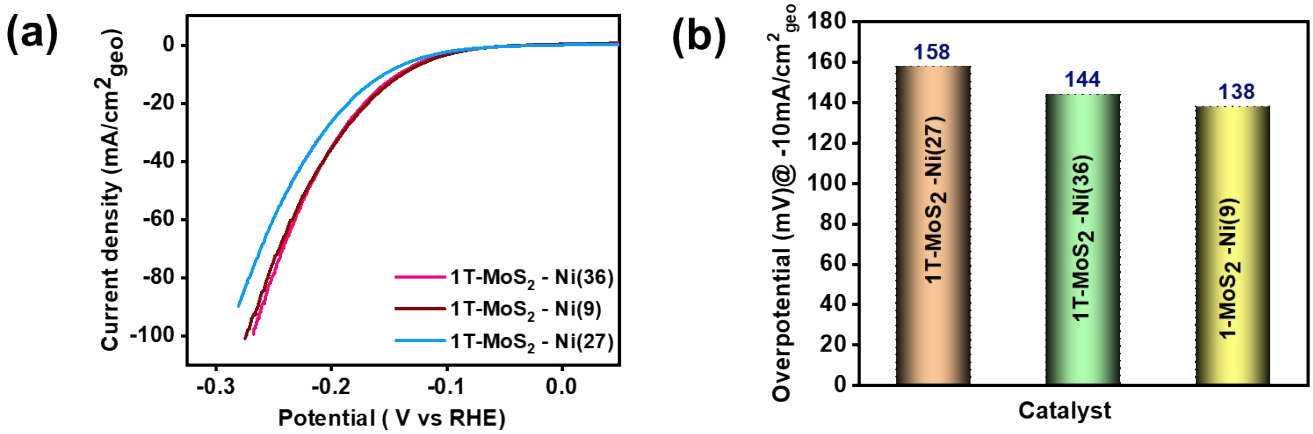

Figure S12: (a) The backward Cathodic polarization curves (100% iR corrected) (recorded at a scan rate of 5 mV/s), (b) Bar diagram representing the overpotential values at -10mA/cm^2_{geo} current density for different 1T-MoS_2-Ni(X) (X = 9, 27, 36) composite materials towards HER in 1M KOH.

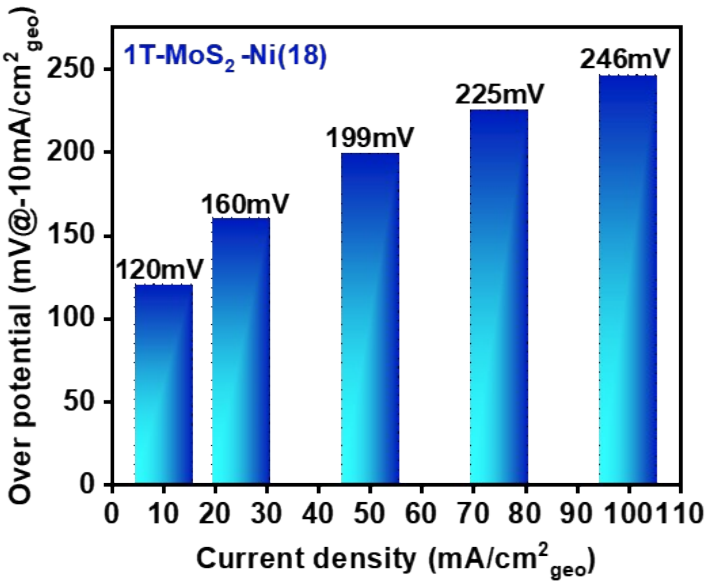

Figure S13: Bar diagram representing the overpotential values for 1T-MoS_2-Ni(18) composite material at different current densities (mA/cm^2_{geo})

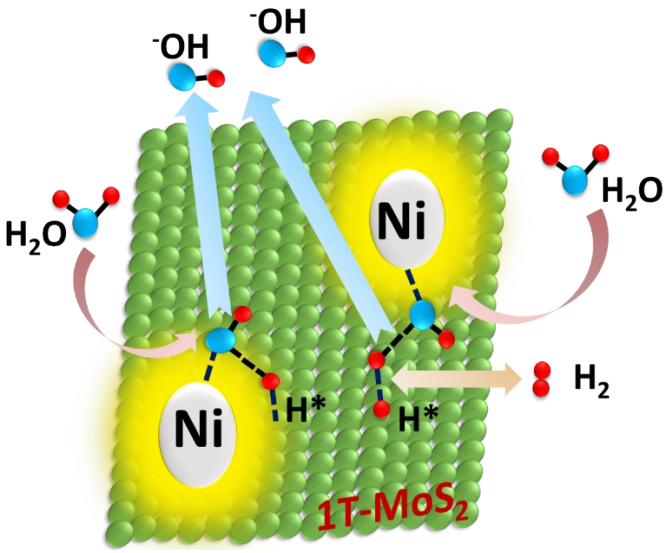

Figure S14: Demonstration of alkaline HER mechanism on 1T-MoS_2 -Ni(X) composite surface, displaying the synergistic effect between metallic Ni and 1T-MoS_2

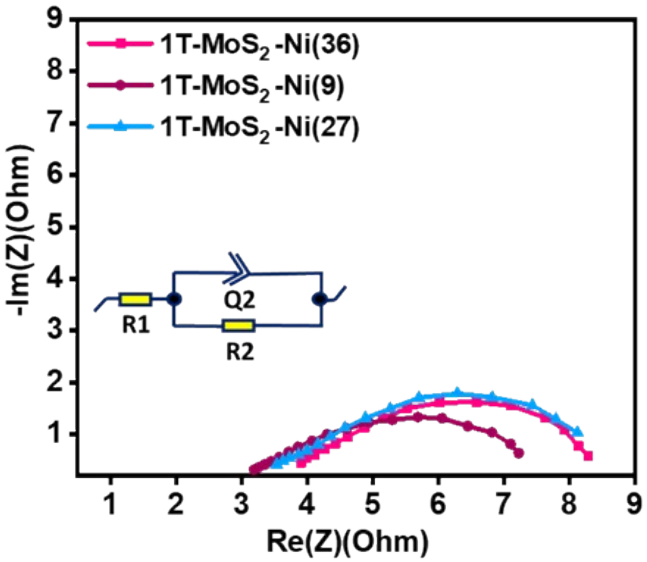

Figure S15: Nyquist plot of 1T-MoS_2-Ni(X) (X = 9, 27, 36) composite materials. Inside the Figure, the corresponding fitted circuit is shown.

Table S2: R_{ct} values of the different as-prepared composite materials.

R2 = R_{ct} (Charge transfer resistance)

Sample Id	1T – MoS_2 – Ni(36)	1T – MoS_2 – Ni(9)	1T – MoS_2 – Ni(27)
R2=R_{ct}	5.2Ω	5.1Ω	6.2Ω

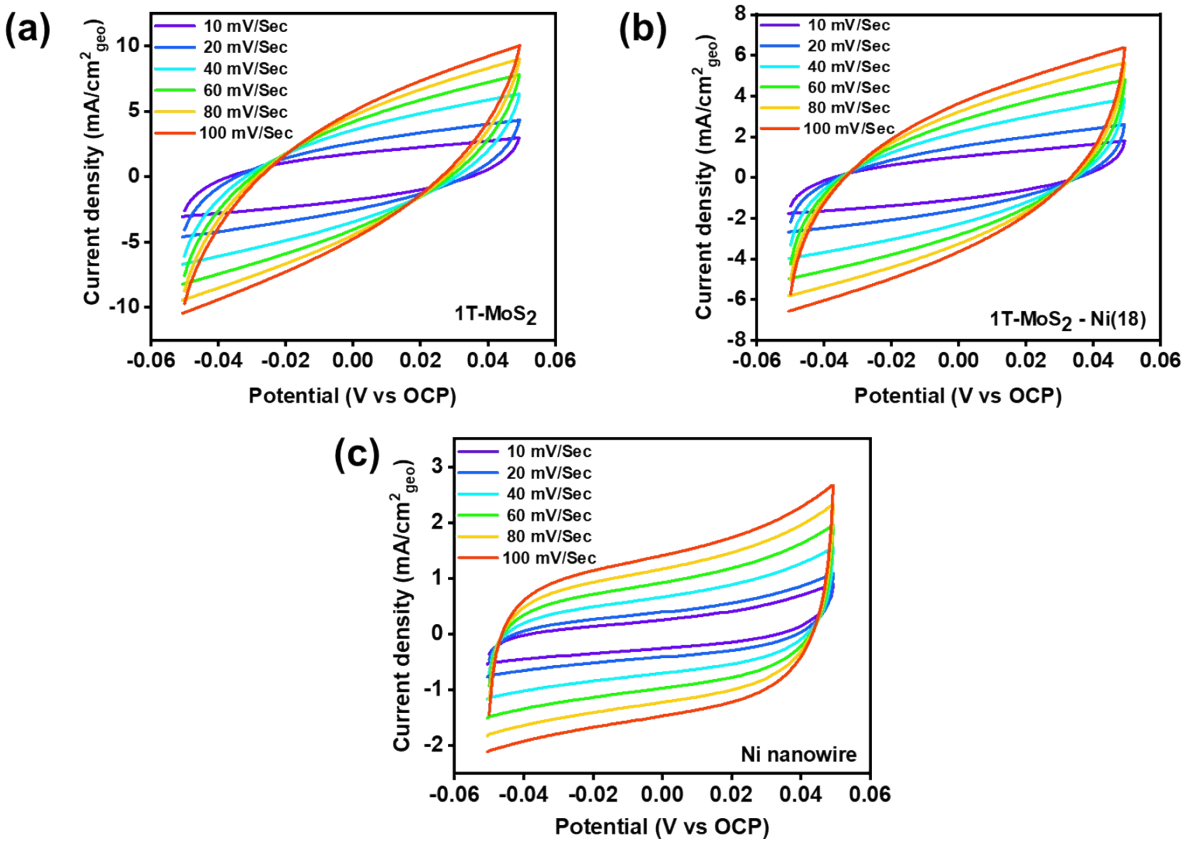

Figure S16: The cyclic voltammograms of (a) 1T-MoS_2 (b) 1T-MoS_2-Ni(18) (c) Ni nanowire recorded at different scan rates to estimate double layer capacitance (C_{dl}) within the potential window of -0.05 V to 0.05 V.

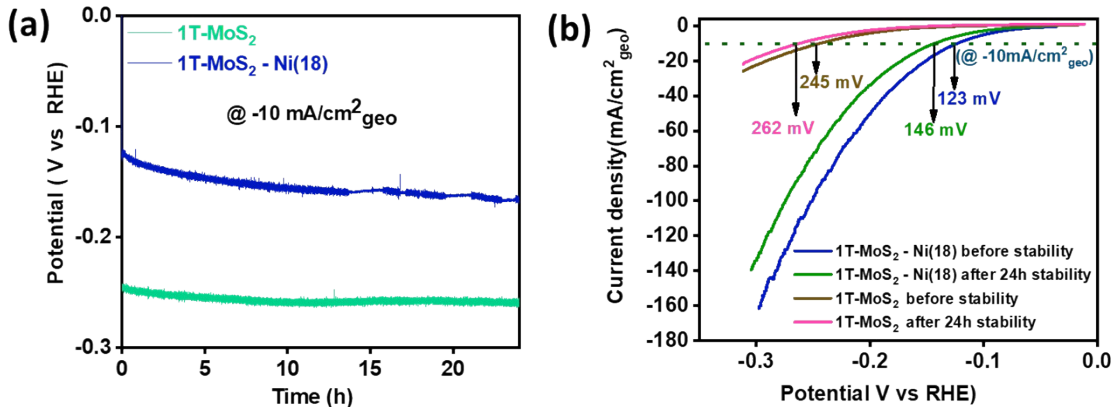

Figure S17: Comparison of stability test (a) chronopotentiometry (CP) (@ 10mA/cm^2_{geo} for 24h), (b) backward LSV curve before and after the CP test of 1T-MoS_2 and 1T-MoS_2 - Ni(18).

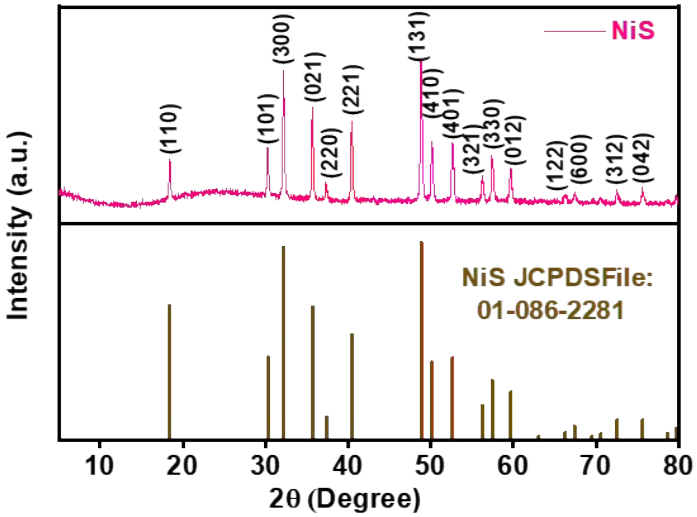

Figure S18: PXRD pattern of as-prepared NiS material with a standard pattern of NiS with JCPDS File: 01-086-2281.

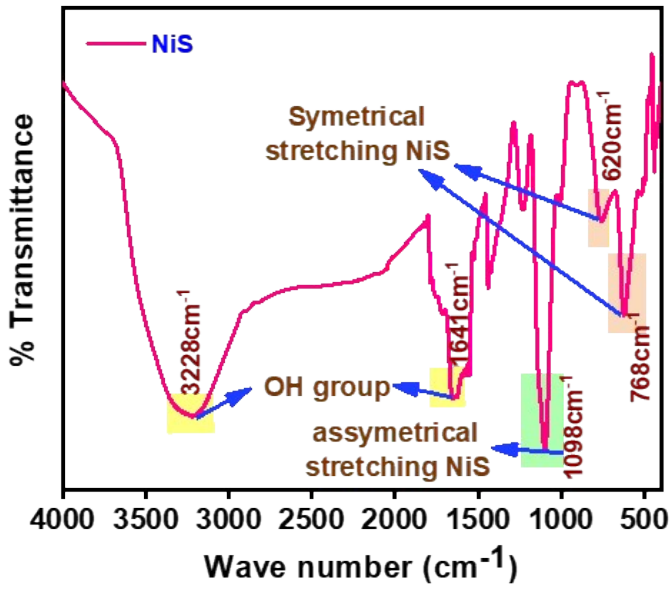

Figure S19: FTIR analysis of as-synthesized NiS material with symmetrical and asymmetrical stretching modes.

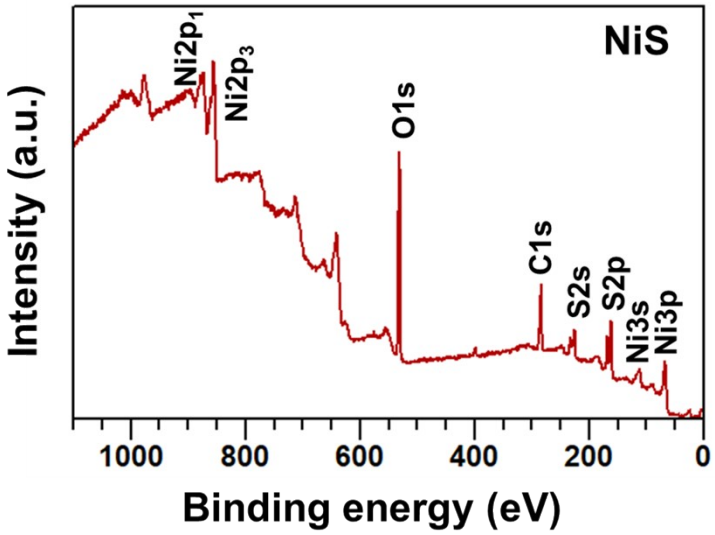

Figure S20: XPS survey scan of as-synthesized NiS.

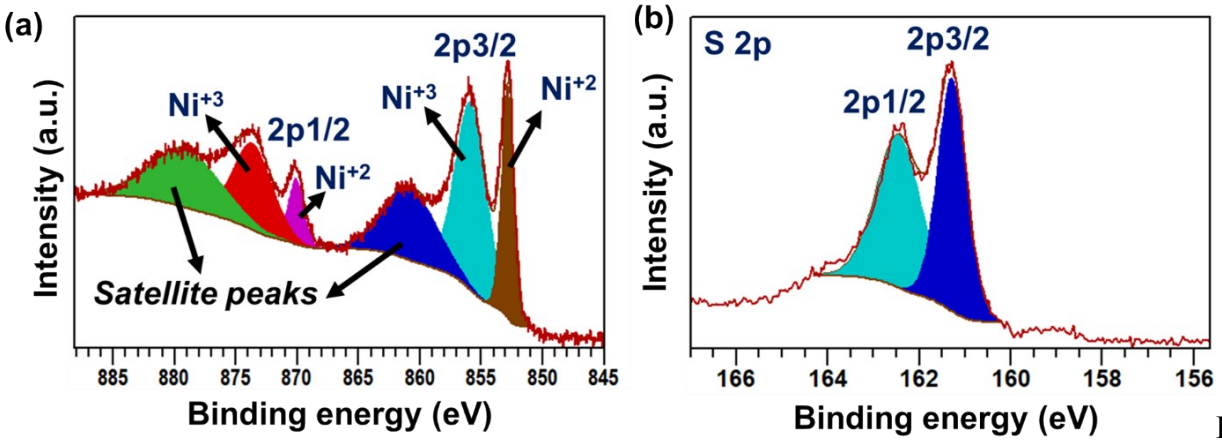

Figure S21: The deconvoluted high-resolution XPS spectra of (a) Ni 2p (b) S 2p of the as prepared NiS material.

Table S3: The XPS peak positions of (a) Ni 2p, (b) S 2p in the as-prepared NiS.

(a)

Element	Ni^{+2}	Ni^{+2}	Ni^{+3}	Ni^{+3}	Satellite	Satellite
Ni (2p)	853eV	870eV	855.8eV	873.6eV	860.8eV	879.1eV

(b)

Element	S 2p3/2	S 2p1/2
S 2p	161.2eV	162.4eV

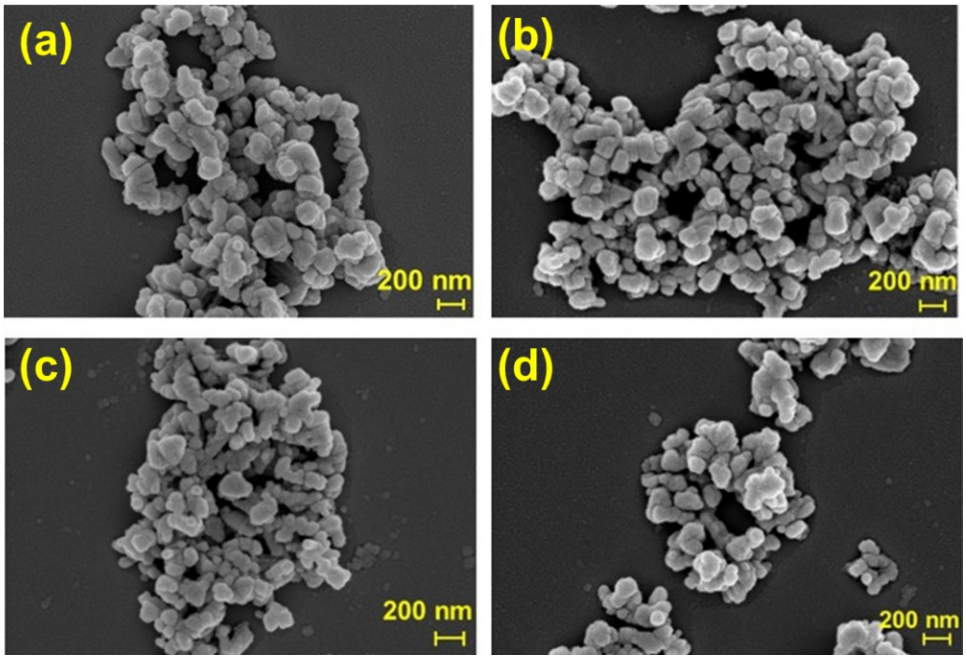

Figure S22: FESEM images of as-prepared NiS material.

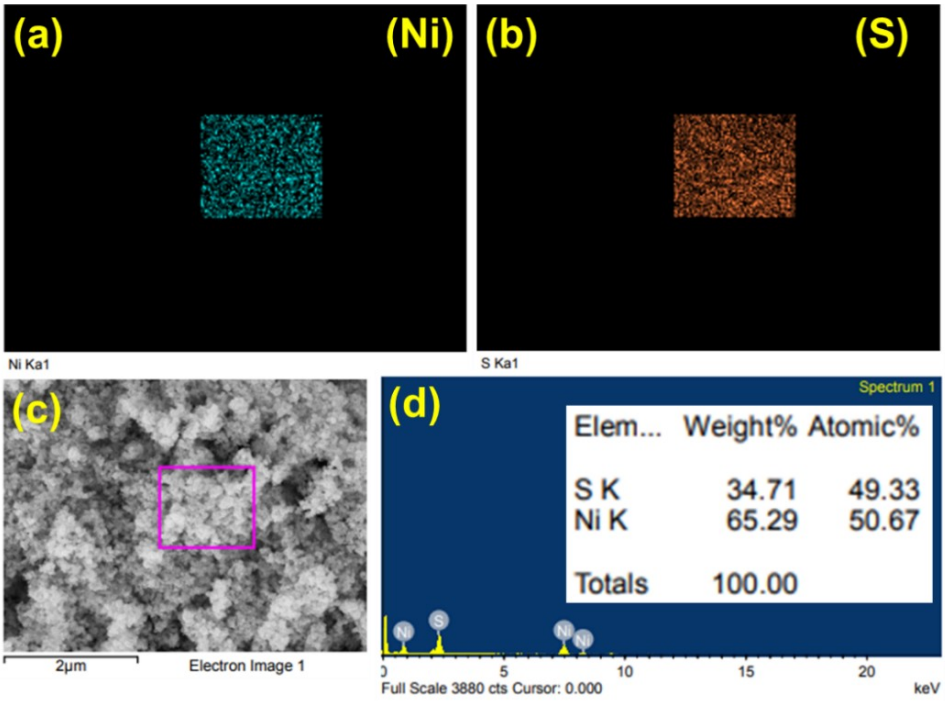

Figure S23: (a, b) Elemental mapping, (c, d) EDS analysis of as-prepared NiS.

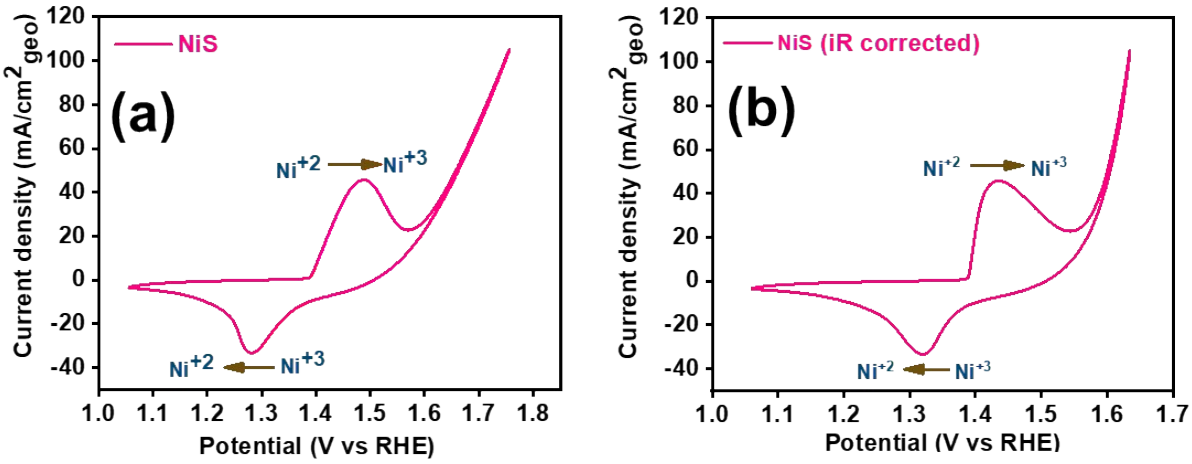

Figure S24: Cyclic Voltammetry curves of (a) without iR correction, (b) after 100% iR correction (recorded at 5mV/s scan rate) for as-prepared NiS material towards alkaline OER in 1M KOH.

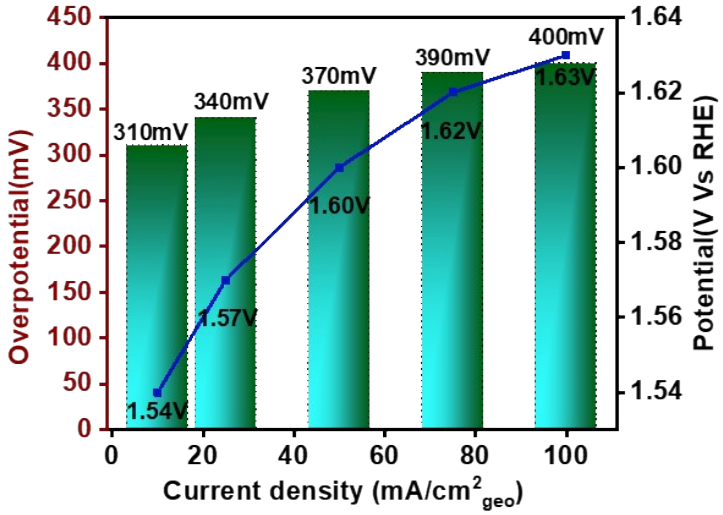

Figure S25: Bar diagram representing the overpotential values as well as the corresponding potential (V vs RHE) at different current densities (mA/cm^2_{geo}) of NiS material towards alkaline OER in 1M KOH.

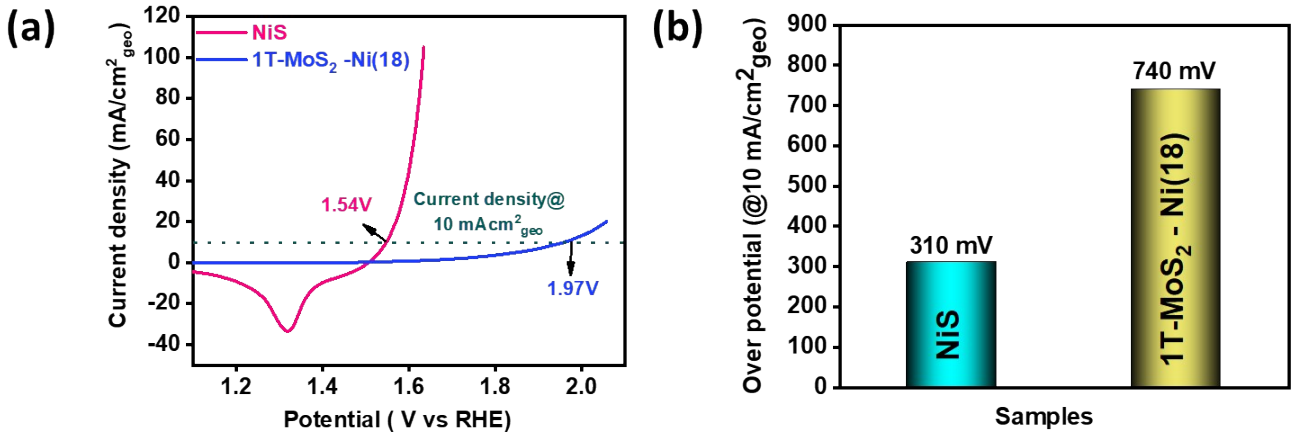

Figure S26 : (a) Backward LSV curve, (b) bar diagram of Overpotential value for NiS and 1T-MoS_2-Ni(18) at 10 mA/cm^2_{geo} towards alkaline OER.

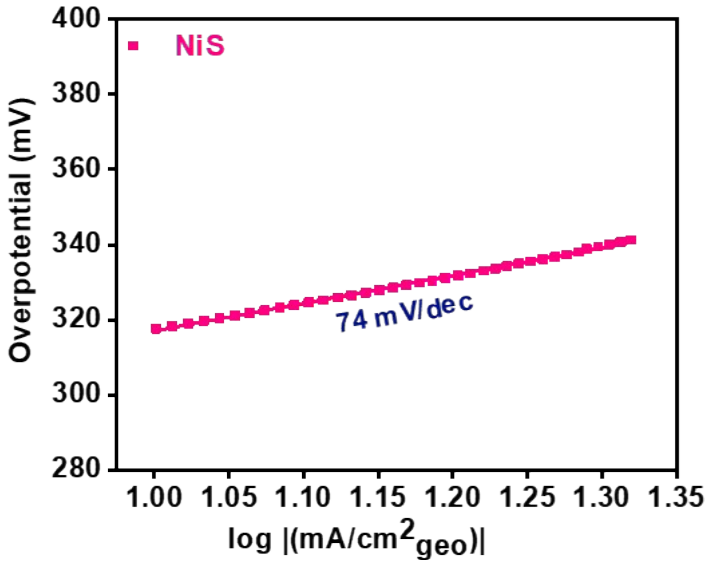

Figure S27: Tafel slope estimation for NiS towards alkaline OER.

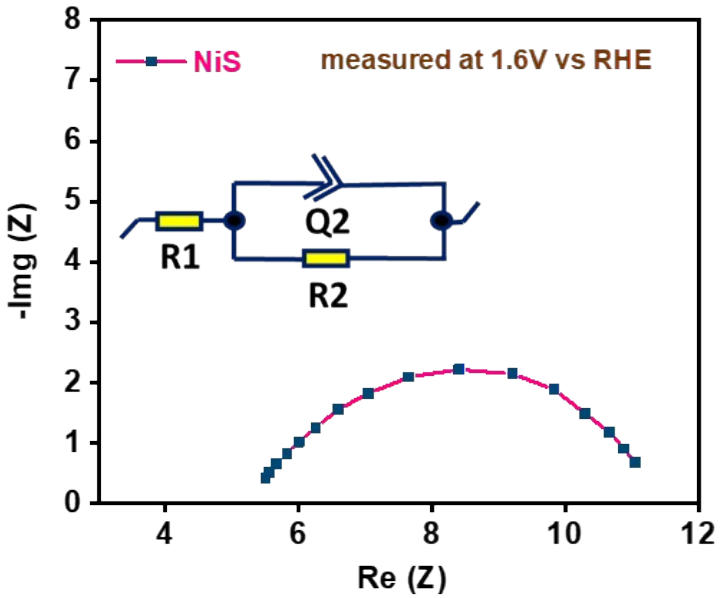

Figure S28: Nyquist plot of NiS towards alkaline OER in 1M KOH. Inside the figure, the corresponding fitting circuit is displayed.

Table S4: Equivalent circuit fitting parameters for corresponding EIS plot of NiS.

Symbol index: **R1**= solution resistance, **R2** = $\mathbf{R_{ct}}$ (Charge transfer resistance), **Q2** = Constant phase element, **a2** = adjustable parameter

R1	Q2	a2	R2
5.4	0.16	0.79	6.0

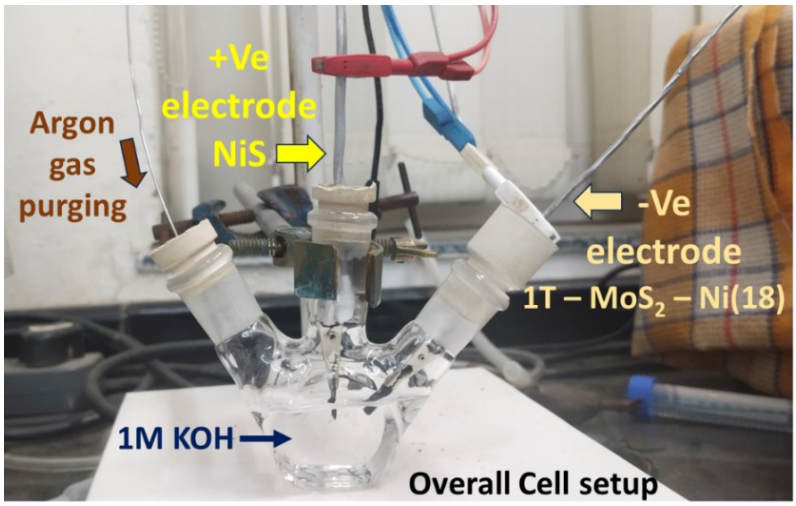

Figure S29: Digital image for a demonstration of alkaline electrolyzer (total water splitting) NiS (+) || 1T-MoS_2-Ni(18) (-)

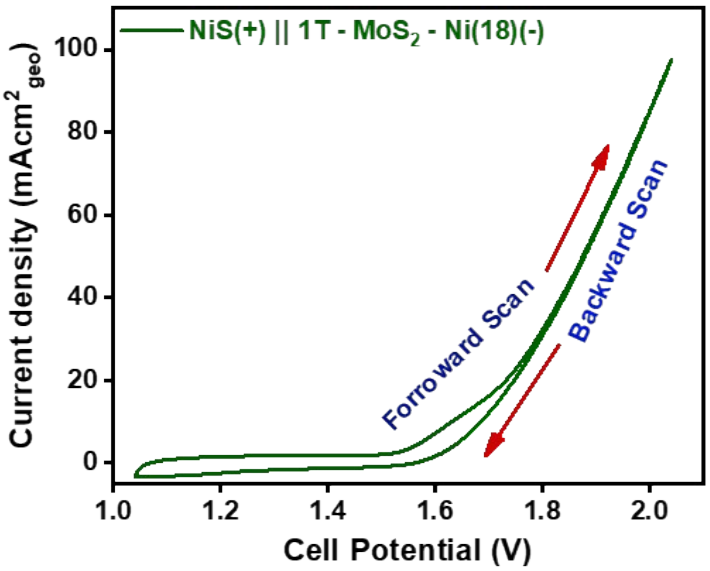

Figure S30: Cyclic Voltammogram of NiS (+) || 1T-MoS_2 –Ni(18) (-) alkaline electrolyser.

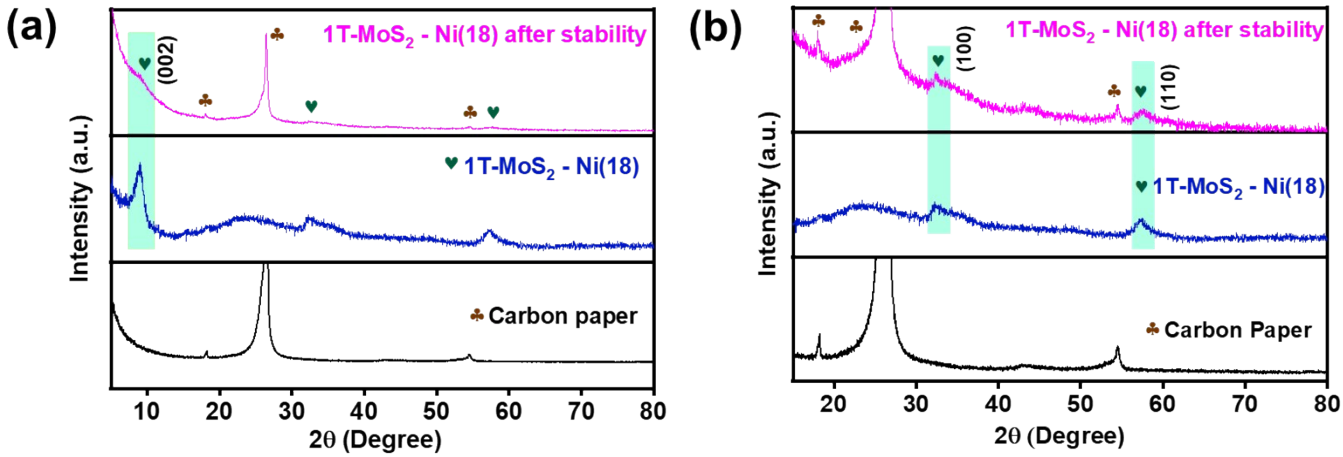

Figure S31: PXRD analysis of 1T-MoS_2-Ni(18) before and after the stability test towards alkaline HER in 1M KOH.

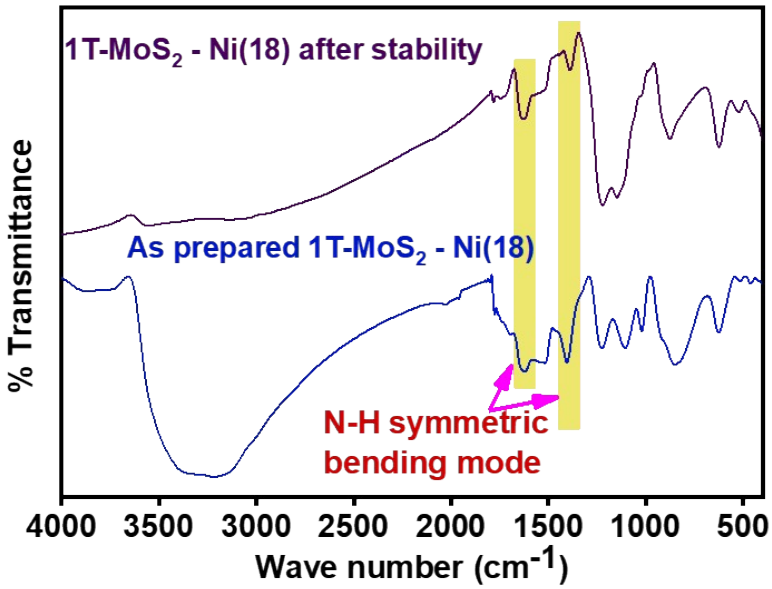

Figure S32: Comparison of FTIR spectra of 1T-MoS_2-Ni(18) before and after the durability test towards HER in 1M KOH.

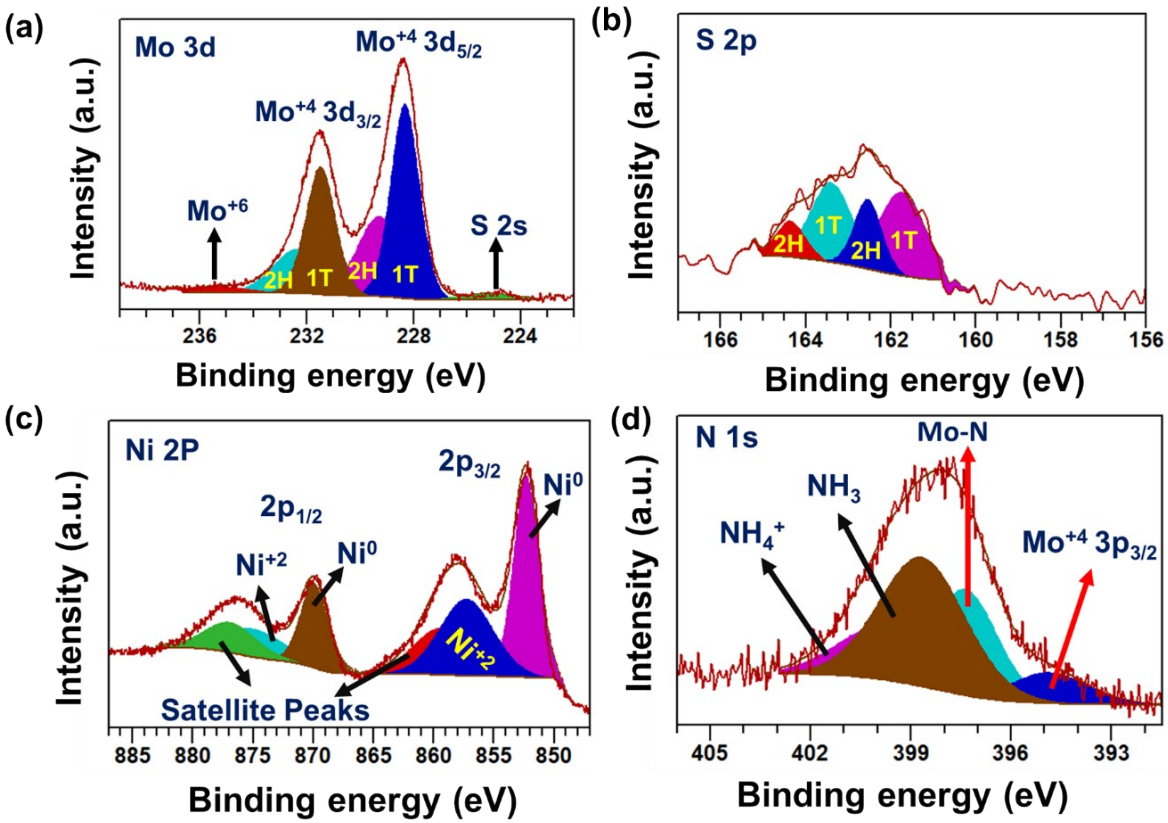

Figure S33: The deconvoluted post-XPS study of (a) Mo 3d, (b) S 2p, (c) Ni 2p, and (d) N 1s of the 1T-MoS_2-Ni(18) composite material towards alkaline HER.

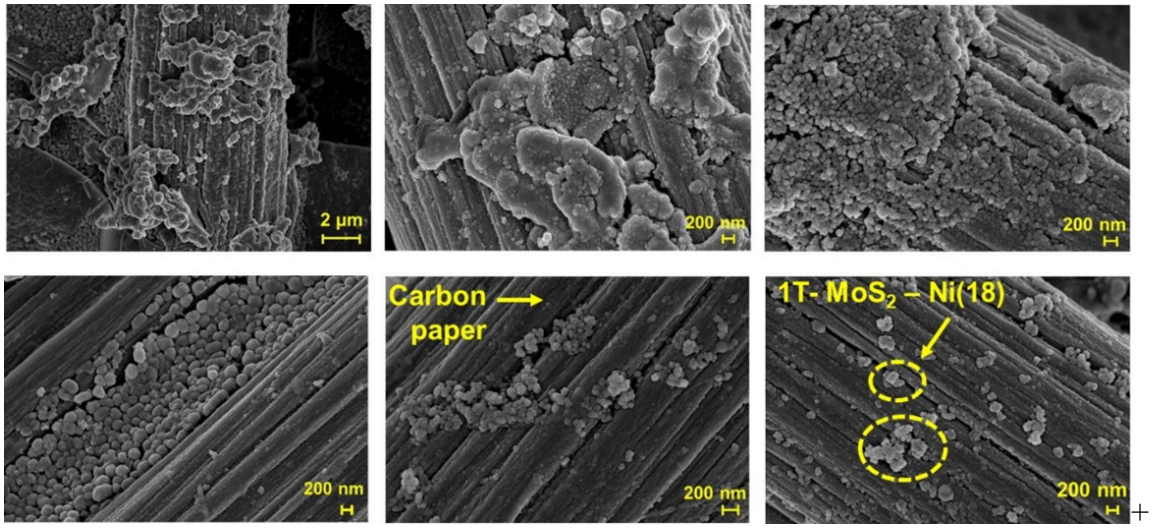

Figure S34: FESEM images of 1T-MoS_2-Ni(18) composite material after the durability test towards HER in 1M KOH.

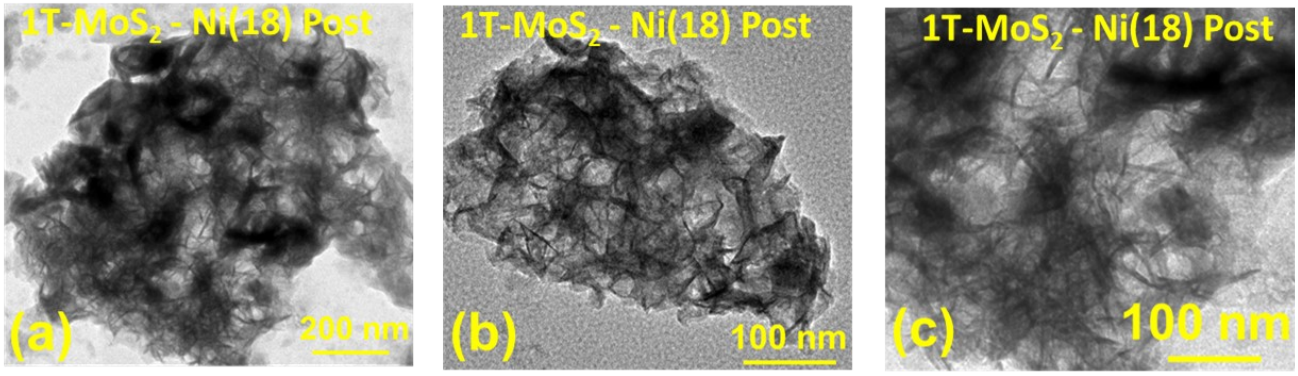

Figure S35: TEM images of 1T-MoS_2-Ni(18) after the durability study towards alkaline HER.

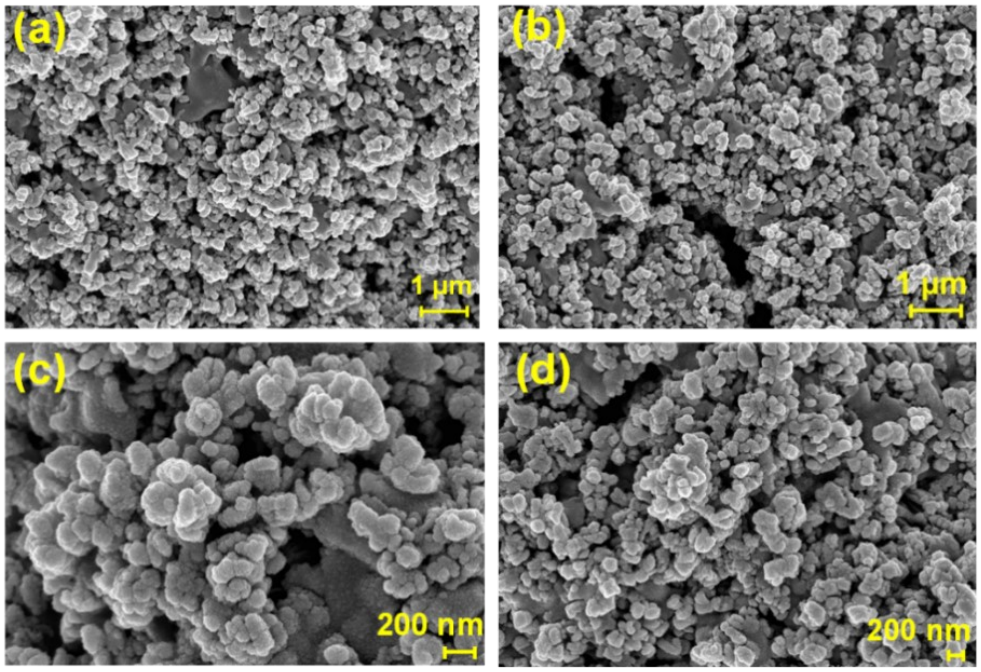

Figure S36: FESEM images of NiS after the stability test towards alkaline OER.

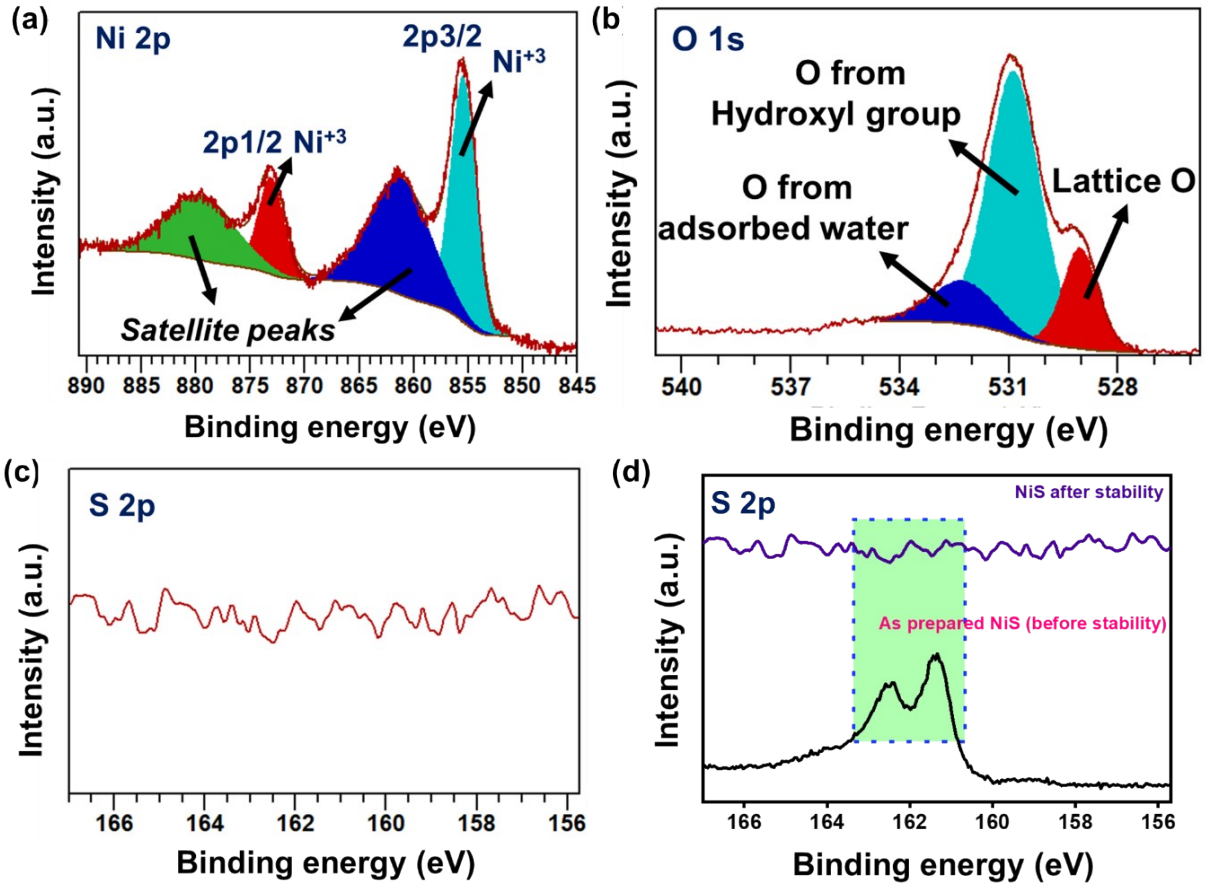

Figure S37: The deconvoluted XPS spectra (a) Ni 2p, (b) O 1s, and (c) S 2p of NiS after the stability test towards alkaline OER. (d) Comparison of sulfur intensity before and after the durability study.

Table S5: The XPS peak positions of (a) Ni 2p, and (b) O 1s for NiS after the stability test.

(a)

Element	Ni^{+3}	Ni^{+3}	Satellite	Satellite
Ni (2p)	855.4 eV	873 eV	861.1eV	879.5eV

(b)

Element	O from adsorbed water	O from hydroxyl group	Lattice O
O 1s	532.2 eV	530.8 eV	529 eV

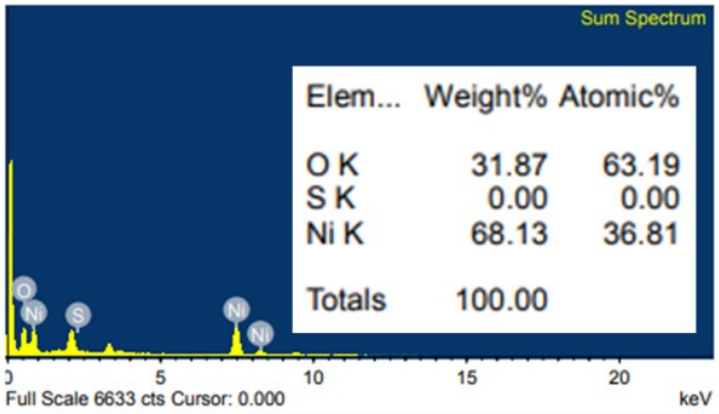

Figure S 38: Post-stability EDS analysis of NiS towards alkaline OER.

Table S6: Overpotential Comparison Table of 1T-MoS_2-Ni(18) composite material with previously reported electrocatalysts towards alkaline HER.

Sl No	Catalyst	Over potential (m V) At 10 mA/cm^2	Electrode substrate and electrode fabrication technique	References
1.	Co doped 1T-MoS_2	118 mV	Carbon Paper (Drop Casting)	(1)
2.	1T-MoS_2/$NiCo_2S_4$	107mV	Carbon Cloth	(2)

			(Direct growth)	
3.	V doped 1T-MoS_2	173mV	Hydrophilic Carbon Paper (Direct growth)	(3)
4.	1T-MoS_2/NiS Heterostructure	120 mV	Ni nanosheet (Direct growth)	(4)
5	Fe/Ni bi-metallic MOF / 1T / 2H MoS_2 heterostructure	140mV	Carbon paper (Drop casting)	(5)
6.	Hatted 1T/2H-Phase MoS_2 - Ni_3S_2 nanorods	73mV	Nickel Foam (Direct growth)	(6)
7.	CoS_2@1T-MoS2 heterostructure	114mV	Carbon cloth (Direct growth)	(7)
8.	Ni/M-MoS_2 (M= metallic)	145mV	Nickel Foam (Drop casting)	(8)
9.	**1T-MoS_2-Ni(18)**	**120mV**	**Carbon paper (Drop casting)**	**This Work**

Reference:

1. H. J. Liu, S. Zhang, Y. M. Chai and B. Dong, *Angew. Chem. Int. Ed.,* 2023, 13845.
2. M. Zheng, Q. Chen and Q. Zhong, *Dalton Transactions*, 2021, **50**, 13320–13328.
3. M. Li, B. Cai, R. Tian, X. Yu, M. B. H. Breese, X. Chu, Z. Han, S. Li, R. Joshi, A. Vinu, T. Wan, Z. Ao, J. Yi and D. Chu, *Chem. Eng. J.*, 2020, **409**, 128158.
4. H. Wei, A. Tan, W. Liu, J. Piao, K. Wan, Z. Liang, Z. Xiang and Z. Fu, *Catalysts*,.2022, **12**, 947
5. Z. Lin, T. Feng, X. Ma and G. Liu, *Fuel*., 2023, **339**, 127395.
6. Y. Zhao, S. Wei, F. Wang, L. Xu, Y. Liu, J. Lin, K. Pan and H. Pang, *Chem. Eur. J.,* 2020, **26**, 2034–2040.
7. Z. Liu, K. Wang, Y. Li, S. Yuan, G. Huang, X. Li and N. Li, *Appl. Catal. B.*, 2021, 120696.
8. N. H. Attanayake, L. Dheer, A. C. Thenuwara, S. C. Abeyweera, C. Collins, U. V. Waghmare and D. R. Strongin, *ChemElectroChem*, 2020, **7**, 3606–3615.